JACS
JOURNAL OF THE AMERICAN CHEMICAL SOCIETY
pubs.acs.org/JACS
Article

Structure Sensitivity of Metal Catalysts Revealed by Interpretable Machine Learning and First-Principles Calculations

Wu Shu, Jiancong Li, Jin-Xun Liu, Chuwei Zhu, Tairan Wang, Li Feng, Runhai Ouyang,* and Wei-Xue Li*

Cite This: J. Am. Chem. Soc. 2024, 146, 8737−8745
Read Online
ACCESS | Metrics & More | Article Recommendations | Supporting Information

ABSTRACT: The nature of the active sites and their structure sensitivity are the keys to rational design of efficient catalysts but have been debated for almost one century in heterogeneous catalysis. Though the Brønsted−Evans−Polanyi (BEP) relationship along with linear scaling relation has long been used to study the reactivity, explicit geometry, and composition properties are absent in this relationship, a fact that prevents its exploration in structure sensitivity of supported catalysts. In this work, based on interpretable multitask symbolic regression and a comprehensive first-principles data set, we discovered a structure descriptor, the topological under-coordinated number mediated by number of valence electrons and the lattice constant, to successfully address the structure sensitivity of metal catalysts. The database used for training, testing, and transferability investigation includes bond-breaking barriers of 20 distinct chemical bonds over 10 transition metals, two metal crystallographic phases, and 17 different facets. The resulting 2D descriptor composing the structure term and the reaction energy term shows great accuracy to predict the reaction barriers and generalizability over the data set with diverse chemical bonds in symmetry, bond order, and steric hindrance. The theory is physical and concise, providing a constructive strategy not only to understand the structure sensitivity but also to decipher the entangled geometric and electronic effects of metal catalysts. The insights revealed are valuable for the rational design of the site-specific metal catalysts.

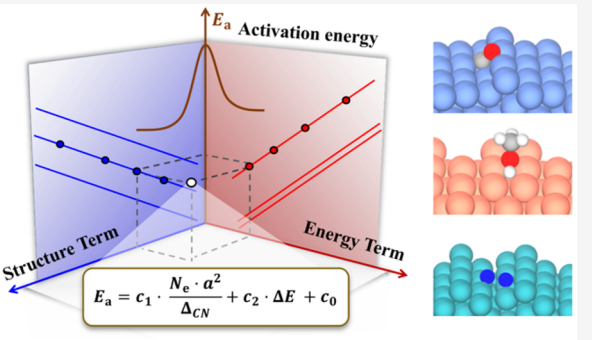

INTRODUCTION

Catalysis plays a pivotal role in a wide range of chemical processes, enabling the synthesis of vital materials and the conversion of raw resources into value-added products.[1,2] In the quest for sustainable and environmentally friendly chemical transformations, the development of efficient catalysts that selectively activate target molecules is of utmost importance.[3−5] Supported transition metals (TMs) are widely used to improve the catalytic activity and selectivity for their great tunability of geometry structure,[6−8] composition,[9,10] size,[11−14] and strong metal−support interaction[15−18] among others. Talyor proposed nearly one century ago that unsaturated active sites control the reactivity,[19] and Boudart classified the catalytic reactions as either structure sensitive or insensitive.[20] Despite great progress so far, considering that there are many factors across multiple scales to contribute to the observed activity and selectivity,[21−25] identification of the intrinsic active sites where the catalysis takes place at the atomic level, its site-specific activity, and structure sensitivity for rational design of efficient catalysts remain a great challenging in heterogeneous catalysis.

The structure sensitivity of metal catalysts is molecule and reaction dependent.[26−28] For instance, the activation of molecular π-bonds requires an active site with a unique configuration of several metal atoms, and the rate of reaction decreases with a decrease of the particle size, whereas the activation of σ-bonds requires the activation to proceed at a single metal atom and the rate increases with a decrease in the particle size.[29,30] In addition, when large-size molecules such as methanol and ethane are considered, the steric effect of the reactants might become pronounced, and its dependence on the particle size changed.[31,32] Moreover, when chemical bonds with different bond order and strength (such as single, double, and triple bonds) are involved, the energy balance between bond breaking and forming at the transition states (TSs) changes as well.[33,34] These distinct chemistries bring multiple variances, which will eventually lead to different structure sensitivities and site-specific activities.

Received: January 31, 2024
Revised: March 7, 2024
Accepted: March 8, 2024
Published: March 14, 2024

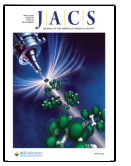

https://doi.org/10.1021/jacs.4c01524
J. Am. Chem. Soc. 2024, 146, 8737−8745

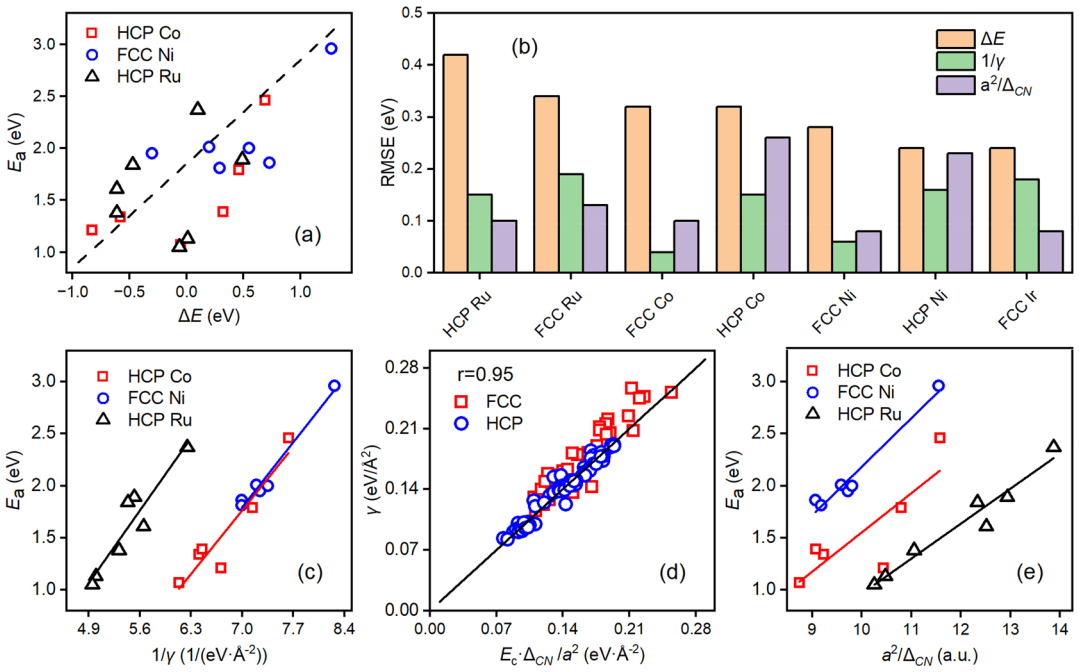

Figure 1. Influence of metal geometry and composition on the CO dissociation. (a) The dissociation barriers of CO against the reaction energy ΔE on various HCP Co, FCC Ni, and HCP Ru surfaces. (b) Comparison of the RMSEs of fitting different physical parameters to the E_a on a variety of transition metal surfaces (data provided in Table S1). (c) E_a against the reciprocal of the surface energy, $1/\gamma$. (d) Comparison between the calculated surface energy γ and that from model $\hat{\gamma}$ in eq 2. (e) E_a against the a^2/Δ_{CN}.

The empirical Bronsted−Evans−Polanyi (BEP) relationship along with the linear scaling relation has long been used as a general theoretical framework to study among others the general trend behavior and influence of the geometric structure and composition of catalysts on activity.[35−38] The BEP relationship correlates the activation energy E_a with the reaction energy ΔE of an elementary reaction,[39−42] that is, $E_a = \alpha\Delta E + \beta$, where α and β are the fitting slope and intercept, respectively. It was believed that the electronic and geometric effects could be separated based on the BEP relationships by α and β, respectively.[43] The BEP relationship holds well for the same class of reaction molecules on different metal surfaces with similar geometric structure where their TSs are the similar and final state-like.[44,45] In this case, ΔE and thus E_a were decided purely by the metal composition (electronic effects). However, when different molecules[44−48] or geometrically distinct surfaces[49,50] were involved, the fitting of the BEP relation to the calculated E_a presents a large error. In fact, in the BEP relationship, the geometry and composition properties of catalysts are not included explicitly, a fact that prevents essentially its exploration in the structure sensitivity and rational design of efficient catalysts.

Recently, machine learning techniques have been used to predict the E_a,[51,52] including linear regression to support vector regression,[53] ensemble tree models,[54] Gaussian processes,[55] and neural networks,[56] just to name a few. When considering the reactants' and surfaces' geometric properties, such as distance, angle, coordination number (CN), bond counts, etc., various models with improved accuracy over the BEP relationship were achieved.[57,58] Though these "black-box" models can reach a higher accuracy, they lack transparency in general.[59] A physically interpretable and concise functional form, explicitly incorporating the composition and geometry properties of catalysts, yet more accurate than the BEP relationship, remains open. Note that, during data mining and machine learning investigation, the generation of a consistent and sufficiently large data set is essential but often hindered here specifically by the high computational cost of TS searching by quantum mechanical calculations. Accordingly, multisource data were often used, and the resulting data heterogeneity brings additional difficulty, which requires the use of proper data-driven approaches.[60]

The above challenges are addressed in this work by using multitask symbolic regression[61] over a comprehensive first-principles bond-breaking barrier data set covering 20 distinct bonds on 10 late transition metals and 17 differently orientated surfaces. Within the framework of Sure Independence Screening and Sparsifying Operator (SISSO)[62,63] and a multitask learning strategy to treat multisource data,[63,64] we build a concise and interpretable site-specific activity descriptor from a huge space of expressions that are a nonlinear combination of the primary composition and geometry features of a metal catalyst. The topologically under-coordinated number (TUCN), mediated by the number of valence electrons and lattice constant of metal catalysts, was discovered to describe successfully the structure sensitivity. This structure term together with the reaction energy term constructs a two-dimensional descriptor, which can predict accurately the reaction barriers of numerous molecules across a broad range of compositions and structures of metal catalysts.

RESULTS AND DISCUSSION

2.1. Geometric Effect of Metal Catalysts. For late transition metals on supports, there are mainly two crystallographic phases: hexagonal close-packed (HCP) and face-centered cubic (FCC). HCP might expose (0001), (10$\bar{1}$0), (10$\bar{1}$1), (10$\bar{1}$2), (11$\bar{2}$0), (11$\bar{2}$1), (20$\bar{2}$1), and (21$\bar{3}$0) facets, whereas FCC might expose (100), (110), (111), (210), (211), (221), (310), (311), and (321) facets. Subjected to the minimization of the overall surface energies and further

https://doi.org/10.1021/jacs.4c01524
J. Am. Chem. Soc. 2024, 146, 8737−8745

influenced by among others the presence of adsorbates, the particle size, and metal−support interaction, exposed facets and their ratio vary. These facets have very different surface geometries, which provide an ideal platform to study the geometry effects as reported below.

Taking CO dissociation as an example, calculated dissociation barriers E_a on various HCP Co and Ru and FCC Ni surfaces are plotted with respect to the reaction energy ΔE in Figure 1a. Though the surfaces with more exothermic ΔE have a lower E_a in general, the linear relationship between E_a and ΔE is hardly seen. Corresponding root mean squared errors (RMSEs) based on the BEP fitting are 0.32, 0.42, and 0.28 eV, respectively, which are too big to predict the reaction rate. When more late transition metals (HCP Ni and FCC Co, Ru, and Ir) (Figure 1b) are considered to add more electronic effects, the corresponding RMSEs are at least 0.24 eV, which remains considerable as well. These show that when different surface structures are concerned, distinct geometric effects break down the BEP relationship. This is expected since the BEP relationship applies best for the surfaces with similar local geometries, where corresponding reaction energies are decided mainly by the composition (electronic effects) and stand out as a single dominating factor.

When different surfaces are involved, corresponding TSs change (Figure S1), and a new descriptor is mandatory to account for the geometric effect. Note that for a given metal the surface with a higher surface energy γ is expected to be more reactive. In the past, we found that for N_2 dissociation on body-centered-cubic (BCC) iron,[65] the higher γ of the surface, the lower the calculated E_a. Inspired by this finding, we plot the E_a of CO dissociation on various HCP Co and Ru and FCC Ni surfaces with respect to the reciprocal of the corresponding γ in Figure 1c. Surprisingly, we find there are very good linear relationships between E_a and $1/\gamma$, as justified by their small RMSEs of 0.15, 0.15, and 0.06 eV, respectively. Even for HCP Ni and FCC Co, Ru, and Ir, their maximum RMSEs remain less than 0.19 eV, as shown in Figure 1b. Alternatively, the RMSEs plotted with respect to $1/\gamma$ are systematically lower than those with respect to ΔE, and for FCC Co they are lowered by as much as 0.28 eV. We also investigated the dissociation of the NO molecule with one more electron in the $2\pi^*$ orbital than CO on various FCC metal surfaces including Co, Ni, Cu, Ru, Rh, Pd, Pt, Ag, and Au. Corresponding RMSEs for E_a versus $1/\gamma$ and ΔE are plotted in Figure S2. Again, the former one shows much better performance than the latter one, lower RMSEs, for instance, by 0.34 eV for Pd and 0.27 eV for Ni. These demonstrate that γ is an excellent descriptor to account for the structural effects of the metal catalysts.

Based on the bond-cutting model, where the bond energy varies with the square root of the coordination number (CN), a surface with lower CN has a higher γ in general.[66−69] Note that for a given surface of interest there might be more than one atom with the same or different CN exposed, and all these atoms with a CN different from the bulk counterpart would raise the surface energy. To account for this, we defined a specific topological under-coordinated number (TUCN), Δ_{CN}, as below:

$$\Delta_{CN} = \frac{a^2}{A}\cdot\sum_{i=1}^{n}\left(1-\sqrt{\frac{N_S^i}{N_B}}\right) \quad (1)$$

where n is the number of exposed atoms in the primitive unit cell with a surface area of A, N_S^i is the corresponding CN of the exposed ith atom, and N_B and a are the bulk CN and lattice constant. The summation counts all exposed metal atoms in the cell. Surface area A is proportional to a^2 and depends further on the crystallography phase and surface orientation. Δ_{CN} is therefore a dimensionless and pure topological geometry variable reflecting the extent of under-coordination. For various facets considered with different surface Miller indexes, corresponding Δ_{CN} are tabulated in Table S2. Specifically, Δ_{CN} are 0.309 and 0.394 for FCC (111) and (110) surfaces and 0.155 and 0.209 for HCP (0001) and $(21\bar{3}0)$, respectively.

We proposed here a generalized model for $\hat{\gamma}$ with respect to Δ_{CN}:

$$\hat{\gamma} = \frac{E_C}{a^2}\cdot\Delta_{CN} \quad (2)$$

where E_C is the cohesive energy of bulk metals, and the prefactor E_C/a^2 is the energy cost to create the surface with respect to the area of a^2. To show the accuracy of eq 2, we considered a total of 101 different surfaces of FCC and HCP metals, including Co, Ni, Cu, Ru, Rh, Pd, Os, and Ir (Table S3). The calculated γ are plotted against the model $\hat{\gamma} = E_C\cdot\Delta_{CN}/a^2$ in Figure 1d, from which an excellent linear relationship (Pearson coefficient $r = 0.95$) can be found.

For a given metal (E_C is fixed), the linear correlation between E_a and a^2/Δ_{CN} could be expected. To show this, we consider CO dissociation on various HCP Co, FCC Ni, and HCP Ru surfaces as mentioned above. The resulting E_a with respect to the a^2/Δ_{CN} are plotted in Figure 1e, from which a good linear relationship is indeed found with RMSEs as small as 0.08 for FCC Ni and 0.10 eV for HCP Ru. Compared to those plots with respect to $1/\gamma$, where HCP Co and FCC Ni overlap considerably (Figure 1c), the corresponding lines are well separated when a^2/Δ_{CN} was used. This shows that the new descriptor is more constructive to differentiate the structure effect. Figure 1b shows the competing accuracy between $1/\gamma$ and a^2/Δ_{CN}, with the averaged RMSEs being ∼0.12 eV for the latter (more data in Table S1). These show that Δ_{CN} is indeed an excellent and better structure descriptor. In the past CN as a descriptor has been used to describe the structure effect on the adsorption energy on a metal surface.[70−74] Compared to the γ applying mainly for the extended systems and/or large-size particles, Δ_{CN} is a local variable. This enables Δ_{CN} to be applied potentially to small-size and finite systems such as nanoparticles and clusters, which requires further investigation. Considering its general application and local characteristics, Δ_{CN} instead of γ is used to describe the geometric effect and site-specific activity of metal catalysts for molecule activations.

2.2. Data-Driven Equation for Structure Sensitivity.

The above result highlights the importance of the Δ_{CN} on activation of the diatomic molecules. To explore statistically how this influences the structural sensitivity and E_a in general, we considered an extensive molecule data set including CO, N_2, NO, NH, OH, CH_xOH_y (x = 1,2, 3,4; y = 0, 1), and CH_xCH_y (x = 0, 1, 2; y = 1, 2, 3). In this data set, diverse chemical bonds with different steric hindrance, bond symmetry, and order/strength are included. In total, 20 different bond-breaking reactions over the above-mentioned nine FCC surfaces and eight HCP surfaces were investigated. To reveal the composition and electronic effects, we looked at 10 late TMs, including Co, Ni, Cu, Ru, Rh, Pd, Ag, Ir, Pt, and Au. As shown schematically in Figure 2, a data set containing

https://doi.org/10.1021/jacs.4c01524
J. Am. Chem. Soc. 2024, 146, 8737−8745

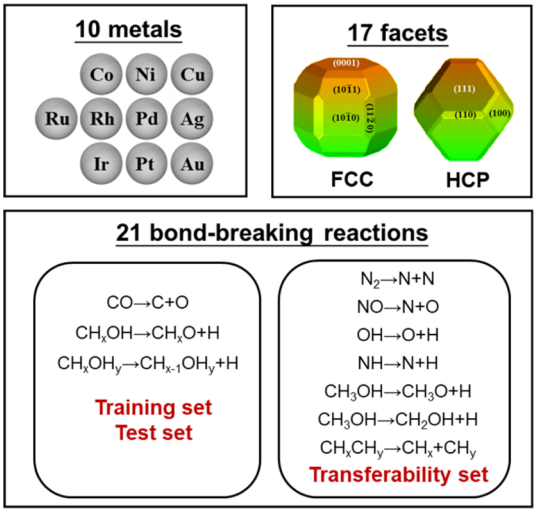

Figure 2. Data sets of the bond-breaking barrier for molecules/radicals on the metal catalysts for multitask symbolic regression. In total, there are 10 transition metals with 17 facets and 20 bond-breading reactions, which were split into the training, test, and transferability sets.

in total 278 barriers E_a are constructed from our own consistent density functional theory (DFT) calculations unless otherwise mentioned (Table S4). The training set for the symbolic regression below includes only C−O, C−H, and O−H bond breaking, while the data set for transferability evaluation involves the N−H, N−N, N−O, and C−C bond breaking, which are completely new to the training set.

We employed multitask symbolic regression within the SISSO (MT-SISSO) to address explicitly the geometric and electronic effects in such a way that high generalizability and high accuracy could be approached simultaneously. In MT-SISSO, all the molecules share the same regression functional form, and each individual molecule was implicitly described by a set of unique coefficients. By means of this, the molecule features and complex steric effects involved in the activation process but hard to describe are reflected in their respective coefficients. The aforementioned Δ_{CN} and 12 physical parameters describing the metal catalysts including the number of valence electrons (N_e), Pauling electronegativity, ionization energy, electron affinity, atomic radius, interplanar distance, and work function were used as input primary features (Table S5) for the symbolic regression. All these primary features are easy to obtain, and the parameters such as the TS structure and the d-band information on the metal, which require explicit DFT calculations, are excluded. Considering the importance of reaction energy in justifying the reaction direction and thermodynamic feasibility, ΔE was included as well in the set of input features.

The goal of identifying the model for E_a should be to have a simple and interpretable functional form yet with high accuracy, e.g., RMSEs around 0.1 eV (the typical level of data noise in DFT calculations). Accordingly, MT-SISSO learning was tested at different dimensions and feature complexity. The results in Figure S3 show that the models at dimension 2 and feature complexity 1 have reached satisfactory accuracy, and the top 10 competing 2D linear models are shown in Table S6. Among these top-ranked models, the feature describing the geometric effect, $1/\Delta_{CN}$, mediated by a prefactor of $N_e \cdot a^2$, appears most frequently in the first term. Interestingly, one of the models has the ΔE naturally emerge as the second term, with the models' form as

$$E_a = c_1 \cdot \frac{N_e \cdot a^2}{\Delta_{CN}} + c_2 \cdot \Delta E + c_0 \quad (3)$$

where c_1, c_2, and c_0 are reaction (task)-specific coefficients, shown in Table S7. We note that the difference of the coefficients between tasks accounts for not only the possible inconsistency between data sources but more importantly the identity of different molecules. Therefore, we did not apply sign constraint in the multitask symbolic regression as proposed in a recent work.[64] Mostly, the coefficients c_1 and c_2 are positive, but negative values (relatively small in magnitude) were also found for a few cases. It is worth noting that the present work is focused on the single-composition catalysts. For alloy catalysts, the weighted N_e and a accounting for the stoichiometry might be required.

The 2D model in eq 3 contains the composition (N_e and a)-mediated geometry term $N_e \cdot a^2/\Delta_{CN}$ (noted as the structure term) and the reaction energy ΔE (noted as the energy term). When the catalyst composition is given, the higher the Δ_{CN} (the more open the surface), the lower the E_a, and the more active the TM, as found above. For a given Δ_{CN}, the structure term shows that E_a increases with N_e and a. In fact, as a rule of thumb, for the late transition metals proceeding from the left to the right along with increases of N_e and from 3d to 5d of the periodic table along with increases of a, corresponding reactivity decreases.[73] The energy term in eq 3 shows the importance of ΔE: the more exothermic the reaction energy is, the lower the activation barrier, as found in the classic BEP relationship. The two terms $N_e \cdot a^2/\Delta_{CN}$ and ΔE account for the composition-mediated structure effect and the reaction energy effect, respectively, and therefore eq 3 will have a better predictive performance, as shown later. Note that not all 2D models could outperform necessarily the BEP model (i.e., 1D). For example, on replacing the structure term by electronegativity, metallic radius, or surface energy, the corresponding RMSEs increase, even up to that of the BEP model (Table S10). Thus, eq 3 combines two essential physical terms along with molecule-specific coefficients to reflect their relative importance to the overall barrier.

The detailed accuracy of eq 3 by using MT-SISSO is shown in Figure 3a, where activations of CO and CH_xOH_y species on various TM surfaces were considered, including totally 96 (40 for the former and 56 for latter) data in training and 15 (7 for the former and 8 for the latter) data in testing, respectively. The resulting training RMSEs of 0.11 eV and mean absolute error (MAE) of 0.09 eV are rather small, whereas the test error increases slightly with RMSEs of 0.18 eV and an MAE of 0.15 eV. We decomposed Figure 3a into 3b and 3c to see the CO and CH_xOH_y data separately. It is seen that the two subsets cover different energy windows with different scattering. Their training and test RMSEs (Figure 3b and 3c) are essentially the same as those in Figure 3a. This exemplifies the robustness and reliability of eq 3, which signify its generalizability to a broad spectrum of molecule bond-breaking processes as addressed below.

To demonstrate the generalizability, we first predict E_a for some bond breaking (N_2 and NO) and radicals (NH and OH) that are unseen in the training and test sets (Figure 2), and the results based on the 2D model versus DFT calculations are plotted in Figure 4a−d. It can be found that the RMSEs are

https://doi.org/10.1021/jacs.4c01524
J. Am. Chem. Soc. 2024, 146, 8737−8745

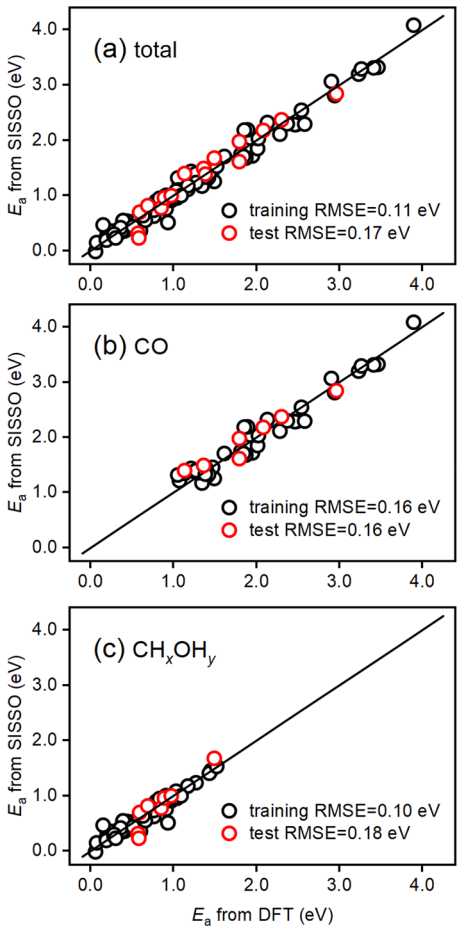

Figure 3. Data-driven eq 3 in plots. (a) Comparison of all the training and test data between the model prediction and DFT calculation. (b and c) Subsets for CO and CH_xOH_y (CH_2OH, CH_3O, CH_2O, CHOH, COH, and CHO), respectively, as extracted from (a).

only 0.15, 0.15, 0.20, and 0.15 eV, respectively, showing excellent accuracy and transferability. For comparison, we calculated their RMSEs based on the BEP model. For N_2 and NO dissociations, the corresponding RMSEs considerably increase by 0.20 eV because of the failure to capture the structure effect, whereas for less structure-sensitive reactions, such as NH and OH bond breaking, corresponding RMSEs of the BEP model increase only by 0.02−0.03 eV. For large and/or polyatomic new molecules with pronounced steric effects, the developed 2D model remains accurate and transferable. To demonstrate this, we considered the CH_3OH and corresponding O−H and C−H bond breaking on various TM surfaces (28 data in total),[76] as well as the CCH, CCH_2, CCH_3, CHCH, $CHCH_2$, $CHCH_3$, CH_2CH_2, and CH_2CH_3 and corresponding C−C bond breaking on various FCC(211) surfaces (47 data in total).[77] Corresponding results are shown in Figure 4e and 4f, and the overall RMSEs are as small as 0.13 and 0.12 eV, respectively. As a comparison, the corresponding RMSEs based on the BEP model are 0.05 and 0.09 eV higher. Considering the exponential influence on the rate, an accurate E_a achieved here is essential.

Concerning the data heterogeneity and its potential influence, we note that the data of E_a were calculated by using different exchange−correlation (xc) functionals,[78] for instance PBE[79] for CO and N_2, RPBE[80] for NO, NH, OH, and CH_xCH_y, and PW91[81] for CH_xOH_y. Detailed calculation parameters can be found in Table S4 and the references therein. Since the present work focused on the surface processes only and there are no calculations of reactants in the gas phase involved, the influence of xc-functionals on corresponding barriers are modest.[15] Moreover, the nature of the multitask learning adopted here treats the different data sources as distinctive tasks for joint feature selection,[60,63] which was demonstrated in a recent work.[64] As a result, the influence arising from the inconsistency of multisource data including but not limited to the xc-functionals is further minimized.

2.3. Entangled Chemistry. The 2D physical model in eq 3 enables us to decipher the composition and geometry effects. As a showcase, we investigated the NO dissociation on four FCC surfaces including (111), (211), (311), and (110) and five TMs including Au, Pd, Cu, Ni, and Co, which were not included in the training set. We first project E_a to $1/\Delta_{CN}$ (Figure 5a). The dependency for each TM is an excellent linear relationship, as indicated by the different and well-separated lines. With an increase of $1/\Delta_{CN}$ from (110) to (111), the E_a increases by ∼0.73 eV for Cu and ∼0.99 eV for Pd, due to their slightly different slopes. The offsets representing different TMs are found to be considerably different and downshift the lines as much as 3.2 eV from Au to Co, which implies a great composition effect. Similarly, we project the value of E_a to ΔE. As shown in Figure 5b, the dependency for each facet is also a linear relationship, as indicated by different but relatively crowded lines. With an increase of ΔE from Co to Au, the E_a increases by 2.25 eV for (111) and 2.53 eV for (211), with slopes varying from 0.67 to 0.62, respectively. The corresponding offsets (or intercept β) representing differently orientated surfaces are found to change relatively modestly. It downshifts the E_a by ∼0.7 eV from the close-packed surface to the open surfaces, but the differences between open surfaces are less than 0.1 eV, in line with previous work.[82,83] This shows again that the structure term introduced is constructive to describe the reactivity across broad composition and geometry space of catalysts.

The physical model developed above allows us to disentangle the contribution from the structure and energy terms, respectively. To demonstrate this, we use NO dissociation as an example to decompose E_a into $c_1 \cdot N_e \cdot a^2/\Delta_{CN}$ and $c_2 \cdot \Delta E$ and plot it in Figure 5c. It can be found that the structure term spans over 2 eV, whereas the energy term about 1 eV only. The two times larger value of the former one shows unambiguously its importance to the overall barrier; namely, the NO dissociation is structure sensitive. For diatomic molecules of CO and N_2, similar results were found as indicated in Figure 5d. Note that in these 2D plots, the corresponding coefficient c_2 of ΔE varies from 0.25 to 0.34, whereas the coefficient α before the ΔE in the BEP relationship varies from 0.60 to 0.82 (Figure 5b and Table S9). The two times larger coefficient indicates that the importance of ΔE might be overestimated in the BEP relationship, in compensating the absence of the explicit structure term. For OH and NH radicals, E_a shows rather weak dependence on the $c_1 \cdot N_e \cdot a^2/\Delta_{CN}$, indicating that these bond breakings are structurally less sensitive. Compared to CO, NO, and N_2, the corresponding coefficient c_1 decreases by a factor of ∼5, whereas c_2 increases by a factor of ∼2 (Tables S8, S9). Accordingly, the influence of the structure term decreases dramatically, and the energy term becomes critical. In this case,

https://doi.org/10.1021/jacs.4c01524
J. Am. Chem. Soc. 2024, 146, 8737−8745

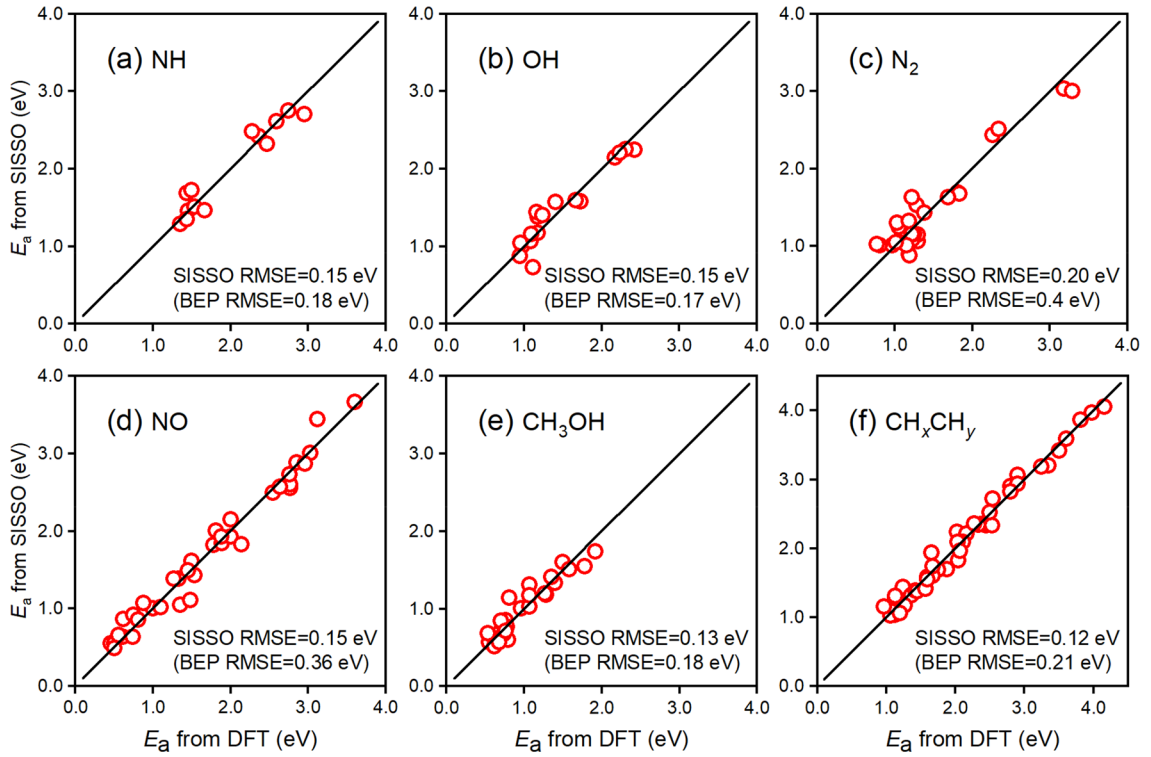

Figure 4. Transferability of eq 3 on unseen species on a variety of metal surfaces. (a) Parity plots for DFT-calculated and the SISSO-model-predicted activation energy E_a of NH. (b–f) The cases for OH, N_2, NO, CH_3OH, and CH_xCH_y, respectively. For comparison, the RMSEs of the BEP prediction are also shown in each panel.

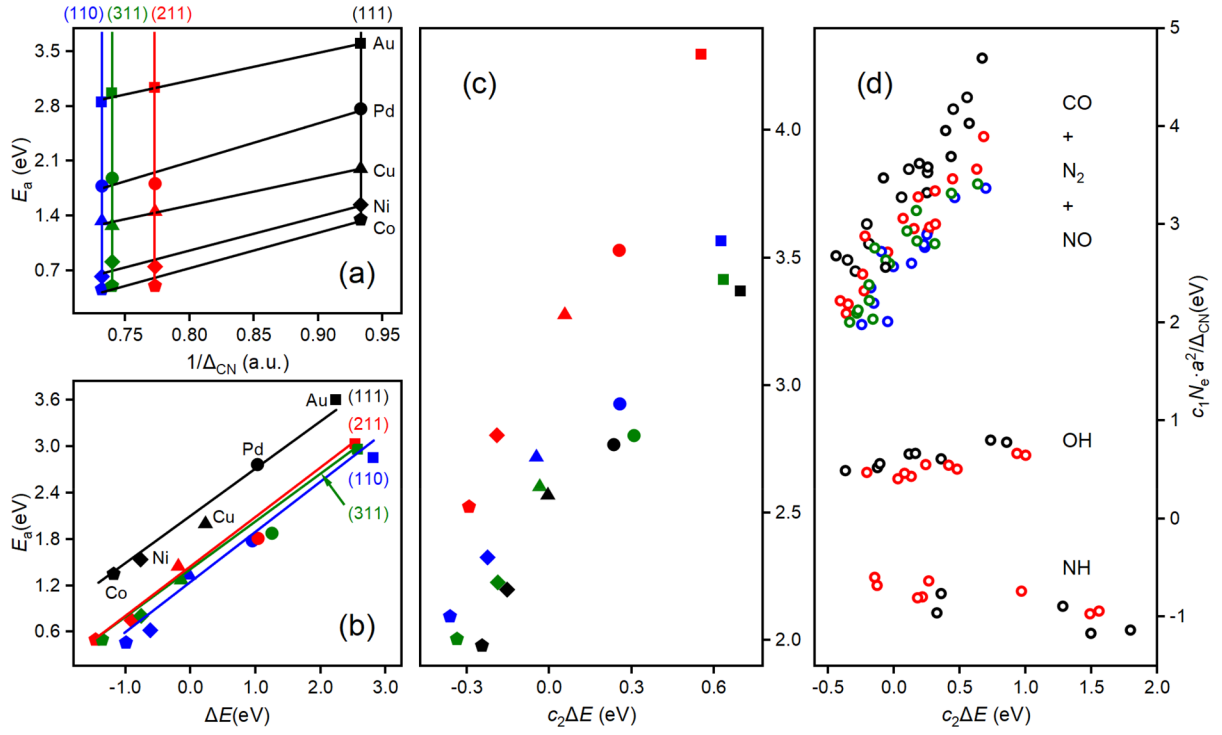

Figure 5. Projection of the activation barrier E_a. (a) NO dissociation E_a against $1/\Delta_{CN}$. Solid symbols: squares (Au), circles (Pd), upward triangles (Cu), diamonds (Ni), and pentagons (Co). Colors: black (111), red (211), green (311), and blue (110). (b) NO dissociation E_a against ΔE. (c) Comparison of the magnitude between $c_1 \cdot N_e \cdot a^2/\Delta_{CN}$ and $c_2 \cdot \Delta E$ for their contributions to the E_a of NO dissociation. (d) Comparison of the magnitude between the two terms for that of NO, CO, N_2, OH, and NH. Colors denote the facets, and the circles denote the collection of available dissociation data on all the considered metal catalysts.

the 2D model behaves like the BEP relationship, and the reactivity is decided mainly by the reaction energy.

In general, for small molecules/radicals, how the reaction barrier are partitioned on the structure term and the energy

https://doi.org/10.1021/jacs.4c01524
J. Am. Chem. Soc. 2024, 146, 8737−8745

term identified above determines the structure sensitivity. A larger projection and coefficient on the former one imply a structure-sensitive reaction, whereas reactions are insensitive with a larger projection and coefficient on the latter. For larger molecules/radicals, where the steric hindrance might play a role, the projection on these two terms and classification of structure sensitivity or insensitivity might not be necessarily clear in physics, but the 2D descriptor identified remains excellent in predicting the reaction barriers.

CONCLUSIONS

By multitask symbolic regression with comprehensive first-principles data, we developed a structure sensitivity theory for metal catalysts that can be applied to a wide range of molecules and radicals. The topological under-coordinated number mediated by the lattice constant and number of valence electron, which is site-specific, is discovered to describe explicitly the structure sensitivity of a metal catalyst. A concise 2D descriptor comprising this structure term and the energy term is developed to predict the reaction barrier. The theory developed provides a constructive strategy not only to classify the structure sensitivity but also to decipher the electronic and geometric effects. The results highlight the importance of transparency of data-driven theory in developing physical models for the rational design of catalysts.

ASSOCIATED CONTENT

Supporting Information

The Supporting Information is available free of charge at https://pubs.acs.org/doi/10.1021/jacs.4c01524.

Method details for the DFT calculations and multitask symbolic regression; transition state structures; model training and validation; RMSEs of fitting the E_a to different physical parameters for diatomic molecules; the Δ_{CN} for different facets; data sets for training, test, and transferability; primary features; the top ranked 10 models; the coefficients for eq 3 (PDF)

The file for data used in machine learning (XLSX)

The file for the atomic coordinates of TS structures (ZIP)

AUTHOR INFORMATION

Corresponding Authors

Runhai Ouyang − *Materials Genome Institute, Shanghai University, Shanghai 200444, China;* orcid.org/0000-0001-9020-0484; Email: rouyang@shu.edu.cn

Wei-Xue Li − *Department of Chemical Physics, Key Laboratory of Precision and Intelligent Chemistry, School of Chemistry and Materials Science and Hefei National Laboratory, University of Science and Technology of China, Hefei 230026, China;* orcid.org/0000-0002-5043-3088; Email: Wxli70@ustc.edu.cn

Authors

Wu Shu − *Department of Chemical Physics, Key Laboratory of Precision and Intelligent Chemistry, School of Chemistry and Materials Science, University of Science and Technology of China, Hefei 230026, China*

Jiancong Li − *Hefei National Research Center for Physical Science at the Microscale, University of Science and Technology of China, Hefei 230026, China*

Jin-Xun Liu − *Department of Chemical Physics, Key Laboratory of Precision and Intelligent Chemistry, School of Chemistry and Materials Science, University of Science and Technology of China, Hefei 230026, China;* orcid.org/0000-0002-7499-4197

Chuwei Zhu − *Hefei National Research Center for Physical Science at the Microscale, University of Science and Technology of China, Hefei 230026, China*

Tairan Wang − *Department of Chemical Physics, Key Laboratory of Precision and Intelligent Chemistry, School of Chemistry and Materials Science, University of Science and Technology of China, Hefei 230026, China*

Li Feng − *Department of Chemical Physics, Key Laboratory of Precision and Intelligent Chemistry, School of Chemistry and Materials Science, University of Science and Technology of China, Hefei 230026, China*

Complete contact information is available at: https://pubs.acs.org/10.1021/jacs.4c01524

Author Contributions

All authors have given approval to the final version of the manuscript.

Notes

The authors declare no competing financial interest.

ACKNOWLEDGMENTS

This work was supported by the National Natural Science Foundation of China (22221003), the Strategic Priority Research Program of the Chinese Academy of Sciences (XDB0450102), Innovation Program for Quantum Science and Technology (2021ZD0303302), K. C. Wong Education (GJTD-2020-15), and the Fundamental Research Funds for the Central Universities (20720220009). The authors also gratefully thank Supercomputing Center of University of Science and Technology of China. R.O. acknowledges the financial support from the National Natural Science Foundation of China (grant no. 22173058). The authors also gratefully thank Supercomputing Center of University of Science and Technology of China.

REFERENCES

(1) Ross, M. B.; De Luna, P.; Li, Y.; Dinh, C.-T.; Kim, D.; Yang, P.; Sargent, E. H. Designing materials for electrochemical carbon dioxide recycling. *Nat. Catal.* **2019**, *2*, 648−658.

(2) Somorjai, G.; Rioux, R. High technology catalysts towards 100% selectivity: Fabrication, characterization and reaction studies. *Catal. Today* **2005**, *100*, 201−215.

(3) Seh, Z. W.; Kibsgaard, J.; Dickens, C. F.; Chorkendorff, I.; Nørskov, J. K.; Jaramillo, T. F. Combining theory and experiment in electrocatalysis: Insights into materials design. *Science* **2017**, *355*, No. eaad4998.

(4) Lazaridou, A.; Smith, L. R.; Pattisson, S.; Dummer, N. F.; Smit, J. J.; Johnston, P.; Hutchings, G. J. Recognizing the best catalyst for a reaction. *Nat. Rev. Chem.* **2023**, *7*, 287−295.

(5) Somorjai, G. A.; Contreras, A. M.; Montano, M.; Rioux, R. M. Clusters, surfaces, and catalysis. *Proc. Natl. Acad. Sci. U. S. A.* **2006**, *103*, 10577−10583.

(6) Honkala, K.; Hellman, A.; Remediakis, I.; Logadottir, A.; Carlsson, A.; Dahl, S.; Christensen, C. H.; Nørskov, J. K. Ammonia synthesis from first-principles calculations. *science* **2005**, *307*, 555−558.

(7) Mavrikakis, M.; Bäumer, M.; Freund, H.-J.; Nørskov, J. K. Structure sensitivity of CO dissociation on Rh surfaces. *Catal. Lett.* **2002**, *81*, 153−156.

(8) Zhu, C. W.; Xu, W. L.; Liu, F.; Luo, J.; Lu, J. L.; Li, W. X. Molecule Saturation Boosts Acetylene Semihydrogenation Activity and Selectivity on a Core-Shell Ruthenium@Palladium Catalyst. *Angew. Chem., Int. Ed.* **2023**, *62*, No. e202300110.
(9) Ruban, A.; Hammer, B.; Stoltze, P.; Skriver, H. L.; Nørskov, J. K. Surface electronic structure and reactivity of transition and noble metals. *J. Mol. Catal. A: Chem.* **1997**, *115*, 421−429.
(10) Norskov, J. K.; Bligaard, T.; Rossmeisl, J.; Christensen, C. H. Towards the computational design of solid catalysts. *Nat. Chem.* **2009**, *1*, 37−46.
(11) Srinivas, S.; Vlachos, D. G. Tuning at the subnanometre scale. *Nat. Catal.* **2022**, *5*, 467−468.
(12) Wang, H.; Gu, X.-K.; Zheng, X.; Pan, H.; Zhu, J.; Chen, S.; Cao, L.; Li, W.-X.; Lu, J. Disentangling the size-dependent geometric and electronic effects of palladium nanocatalysts beyond selectivity. *Sci. Adv.* **2019**, *5*, No. eaat6413.
(13) Cao, S.; Tao, F. F.; Tang, Y.; Li, Y.; Yu, J. Size-and shape-dependent catalytic performances of oxidation and reduction reactions on nanocatalysts. *Chem. Soc. Rev.* **2016**, *45*, 4747−4765.
(14) Liu, L.; Corma, A. Metal catalysts for heterogeneous catalysis: from single atoms to nanoclusters and nanoparticles. *Chem. Rev.* **2018**, *118*, 4981−5079.
(15) Hu, S.; Li, W.-X. Sabatier principle of metal-support interaction for design of ultrastable metal nanocatalysts. *Science* **2021**, *374*, 1360−1365.
(16) Matsubu, J. C.; Zhang, S.; DeRita, L.; Marinkovic, N. S.; Chen, J. G.; Graham, G. W.; Pan, X.; Christopher, P. Adsorbate-mediated strong metal−support interactions in oxide-supported Rh catalysts. *Nat. Chem.* **2017**, *9*, 120−127.
(17) Luo, Z.; Zhao, G.; Pan, H.; Sun, W. Strong metal−support interaction in heterogeneous catalysts. *Adv. Energy Mater.* **2022**, *12*, No. 2201395.
(18) Gu, J.; Jian, M.; Huang, L.; Sun, Z.; Li, A.; Pan, Y.; Yang, J.; Wen, W.; Zhou, W.; Lin, Y.; et al. Synergizing metal−support interactions and spatial confinement boosts dynamics of atomic nickel for hydrogenations. *Nat. Nanotechnol.* **2021**, *16*, 1141−1149.
(19) Taylor, H. S.; Armstrong, E. F. A theory of the catalytic surface. *Proc. R. Soc. London Ser. A-Math. Phys. Eng. Sci.* **1925**, *108*, 105−111.
(20) Boudart, M. Catalysis by supported metals. *Adv. Catal.* **1969**, *20*, 153−166.
(21) Liu, J. X.; Su, H. Y.; Sun, D. P.; Zhang, B. Y.; Li, W. X. Crystallographic dependence of CO activation on cobalt catalysts: HCP versus FCC. *J. Am. Chem. Soc.* **2013**, *135*, 16284−7.
(22) Vogt, C.; Weckhuysen, B. M. The concept of active site in heterogeneous catalysis. *Nat. Rev. Chem.* **2022**, *6*, 89−111.
(23) Behrens, M.; Studt, F.; Kasatkin, I.; Kühl, S.; Hävecker, M.; Abild-Pedersen, F.; Zander, S.; Girgsdies, F.; Kurr, P.; Kniep, B.-L.; et al. The active site of methanol synthesis over Cu/ZnO/Al2O3 industrial catalysts. *Science* **2012**, *336*, 893−897.
(24) Li, H.; Li, Y.; Koper, M. T. M.; Calle-Vallejo, F. Bond-Making and Breaking between Carbon, Nitrogen, and Oxygen in Electrocatalysis. *J. Am. Chem. Soc.* **2014**, *136*, 15694−15701.
(25) Liu, Z.-P.; Hu, P. General rules for predicting where a catalytic reaction should occur on metal surfaces: a density functional theory study of C− H and C− O bond breaking/making on flat, stepped, and kinked metal surfaces. *J. Am. Chem. Soc.* **2003**, *125*, 1958−1967.
(26) Koper, M. T. Structure sensitivity and nanoscale effects in electrocatalysis. *Nanoscale* **2011**, *3*, 2054−2073.
(27) Lim, J.; Liu, C.-Y.; Park, J.; Liu, Y.-H.; Senftle, T. P.; Lee, S. W.; Hatzell, M. C. Structure sensitivity of Pd facets for enhanced electrochemical nitrate reduction to ammonia. *ACS Catal.* **2021**, *11*, 7568−7577.
(28) Zhang, H.; Jin, M. S.; Xiong, Y. J.; Lim, B.; Xia, Y. N. Shape-Controlled Synthesis of Pd Nanocrystals and Their Catalytic Applications. *Acc. Chem. Res.* **2013**, *46*, 1783−1794.
(29) Che, M.; Bennett, C. O. The influence of particle size on the catalytic properties of supported metals. *Adv. Catal.* **1989**, *36*, 55−172.
(30) Van Santen, R. A. Complementary Structure Sensitive and Insensitive Catalytic Relationships. *Acc. Chem. Res.* **2009**, *42*, 57−66.
(31) Zhao, Y. H.; Liu, J. X.; Su, H. Y.; Sun, K.; Li, W. X. A First-Principles Study of Carbon−Oxygen Bond Scission in Multiatomic Molecules on Flat and Stepped Metal Surfaces. *ChemCatChem.* **2014**, *6*, 1755−1762.
(32) Guo, Y.; Wang, M.; Zhu, Q.; Xiao, D.; Ma, D. Ensemble effect for single-atom, small cluster and nanoparticle catalysts. *Nat. Catal.* **2022**, *5*, 766−776.
(33) Pettersson, L. G. M.; Nilsson, A. A Molecular Perspective on the d-Band Model: Synergy Between Experiment and Theory. *Top. Catal.* **2014**, *57*, 2−13.
(34) Latimer, A. A.; Kulkarni, A. R.; Aljama, H.; Montoya, J. H.; Yoo, J. S.; Tsai, C.; Abild-Pedersen, F.; Studt, F.; Norskov, J. K. Understanding trends in C-H bond activation in heterogeneous catalysis. *Nat. Mater.* **2017**, *16*, 225−229.
(35) Pérez-Ramírez, J.; López, N. Strategies to break linear scaling relationships. *Nat. Catal.* **2019**, *2*, 971−976.
(36) Motagamwala, A. H.; Ball, M. R.; Dumesic, J. A. Microkinetic Analysis and Scaling Relations for Catalyst Design. *Annu. Rev. Chem. Biomol. Engineer.* **2018**, *9*, 413−450.
(37) Zhao, Z.-J.; Liu, S.; Zha, S.; Cheng, D.; Studt, F.; Henkelman, G.; Gong, J. Theory-guided design of catalytic materials using scaling relationships and reactivity descriptors. *Nat. Rev. Mater.* **2019**, *4*, 792−804.
(38) Greeley, J. Theoretical Heterogeneous Catalysis: Scaling Relationships and Computational Catalyst Design. *Annu. Rev. Chem. Biomol. Engineer.* **2016**, *7*, 605−635.
(39) Liu, Z.-P.; Hu, P. General trends in CO dissociation on transition metal surfaces. *J. Chem. Phys.* **2001**, *114*, 8244−8247.
(40) Nørskov, J. K.; Bligaard, T.; Logadottir, A.; Bahn, S.; Hansen, L. B.; Bollinger, M.; Bengaard, H.; Hammer, B.; Sljivancanin, Z.; Mavrikakis, M.; et al. Universality in heterogeneous catalysis. *J. Catal.* **2002**, *209*, 275−278.
(41) Logadottir, A.; Rod, T. H.; Nørskov, J. K.; Hammer, B.; Dahl, S.; Jacobsen, C. The Brønsted−Evans−Polanyi relation and the volcano plot for ammonia synthesis over transition metal catalysts. *J. Catal.* **2001**, *197*, 229−231.
(42) Michaelides, A.; Liu, Z.-P.; Zhang, C.; Alavi, A.; King, D. A.; Hu, P. Identification of general linear relationships between activation energies and enthalpy changes for dissociation reactions at surfaces. *J. Am. Chem. Soc.* **2003**, *125*, 3704−3705.
(43) Norskov, J. K.; Bligaard, T.; Hvolbæk, B.; Abild-Pedersen, F.; Chorkendorff, I.; Christensen, C. H. The nature of the active site in heterogeneous metal catalysis. *Chem. Soc. Rev.* **2008**, *37*, 2163−2171.
(44) Wang, S.; Vorotnikov, V.; Sutton, J. E.; Vlachos, D. G. Brønsted−Evans−Polanyi and Transition State Scaling Relations of Furan Derivatives on Pd(111) and Their Relation to Those of Small Molecules. *ACS Catal.* **2014**, *4*, 604−612.
(45) Sutton, J. E.; Vlachos, D. G. A Theoretical and Computational Analysis of Linear Free Energy Relations for the Estimation of Activation Energies. *ACS Catal.* **2012**, *2*, 1624−1634.
(46) Sutton, J. E.; Vlachos, D. G. Effect of errors in linear scaling relations and Brønsted−Evans−Polanyi relations on activity and selectivity maps. *J. Catal.* **2016**, *338*, 273−283.
(47) Wang, S.; Temel, B.; Shen, J.; Jones, G.; Grabow, L. C.; Studt, F.; Bligaard, T.; Abild-Pedersen, F.; Christensen, C. H.; Nørskov, J. K. Universal Brønsted-Evans-Polanyi Relations for C−C, C−O, C−N, N−O, N−N, and O−O Dissociation Reactions. *Catal. Lett.* **2011**, *141*, 370−373.
(48) Zaffran, J. r. m.; Michel, C.; Delbecq, F. o.; Sautet, P. Trade-off between accuracy and universality in linear energy relations for alcohol dehydrogenation on transition metals. *J. Phys. Chem. C* **2015**, *119*, 12988−12998.
(49) Wang, S.; Petzold, V.; Tripkovic, V.; Kleis, J.; Howalt, J. G.; Skulason, E.; Fernández, E.; Hvolbæk, B.; Jones, G.; Toftelund, A.; et al. Universal transition state scaling relations for (de) hydrogenation over transition metals. *Phys. Chem. Chem. Phys.* **2011**, *13*, 20760−20765.

https://doi.org/10.1021/jacs.4c01524
J. Am. Chem. Soc. 2024, 146, 8737−8745

(50) Wang, S.; Petzold, V.; Tripkovic, V.; Kleis, J.; Howalt, J. G.; Skulason, E.; Fernandez, E. M.; Hvolbaek, B.; Jones, G.; Toftelund, A.; Falsig, H.; Bjorketun, M.; Studt, F.; Abild-Pedersen, F.; Rossmeisl, J.; Norskov, J. K.; Bligaard, T. Universal transition state scaling relations for (de)hydrogenation over transition metals. *Phys. Chem. Chem. Phys.* **2011**, *13*, 20760−5.
(51) Gu, G. H.; Choi, C.; Lee, Y.; Situmorang, A. B.; Noh, J.; Kim, Y. H.; Jung, Y. Progress in Computational and Machine-Learning Methods for Heterogeneous Small-Molecule Activation. *Adv. Mater.* **2020**, *32*, No. e1907865.
(52) Xu, J.; Cao, X.-M.; Hu, P. Perspective on computational reaction prediction using machine learning methods in heterogeneous catalysis. *Phys. Chem. Chem. Phys.* **2021**, *23*, 11155−11179.
(53) Takahashi, K.; Miyazato, I. Rapid estimation of activation energy in heterogeneous catalytic reactions via machine learning. *J. Comput. Chem.* **2018**, *39*, 2405−2408.
(54) Hutton, D. J.; Cordes, K. E.; Michel, C.; Göltl, F. Machine Learning-Based Prediction of Activation Energies for Chemical Reactions on Metal Surfaces. *J. Chem. Inf. Model.* **2023**, *63*, 6006−6013.
(55) Abdelfatah, K.; Yang, W.; Vijay Solomon, R.; Rajbanshi, B.; Chowdhury, A.; Zare, M.; Kundu, S. K.; Yonge, A.; Heyden, A.; Terejanu, G. Prediction of transition-state energies of hydrodeoxygenation reactions on transition-metal surfaces based on machine learning. *J. Phys. Chem. C* **2019**, *123*, 29804−29810.
(56) Wang, B.; Gu, T.; Lu, Y.; Yang, B. Prediction of energies for reaction intermediates and transition states on catalyst surfaces using graph-based machine learning models. *Mol. Catal.* **2020**, *498*, No. 111266.
(57) Xu, J.; Cao, X.-M.; Hu, P. Improved Prediction for the Methane Activation Mechanism on Rutile Metal Oxides by a Machine Learning Model with Geometrical Descriptors. *J. Phys. Chem. C* **2019**, *123*, 28802−28810.
(58) Singh, A. R.; Rohr, B. A.; Gauthier, J. A.; Nørskov, J. K. Predicting Chemical Reaction Barriers with a Machine Learning Model. *Catal. Lett.* **2019**, *149*, 2347−2354.
(59) Esterhuizen, J. A.; Goldsmith, B. R.; Linic, S. Interpretable machine learning for knowledge generation in heterogeneous catalysis. *Nat. Catal.* **2022**, *5*, 175−184.
(60) Thung, K.-H.; Wee, C.-Y. A brief review on multi-task learning. *Multimed. Tools Appl.* **2018**, *77*, 29705−29725.
(61) Wang, Y.; Wagner, N.; Rondinelli, J. M. Symbolic regression in materials science. *MRS Commun.* **2019**, *9*, 793−805.
(62) Ouyang, R.; Curtarolo, S.; Ahmetcik, E.; Scheffler, M.; Ghiringhelli, L. SISSO: A compressed-sensing method for identifying the best low-dimensional descriptor in an immensity of offered candidates. *Phys. Rev. Mater.* **2018**, *2*, No. 083802.
(63) Ouyang, R. H.; Ahmetcik, E.; Carbogno, C.; Scheffler, M.; Ghiringhelli, L. M. Simultaneous learning of several materials properties from incomplete databases with multi-task SISSO. *J. Phys-Mater.* **2019**, *2*, No. 024002.
(64) Wang, J.; Xie, H.; Wang, Y.; Ouyang, R. Distilling Accurate Descriptors from Multi-Source Experimental Data for Discovering Highly Active Perovskite OER Catalysts. *J. Am. Chem. Soc.* **2023**, *145*, 11457−11465.
(65) Zhang, B. Y.; Su, H. Y.; Liu, J. X.; Li, W. X. Interplay Between Site Activity and Density of BCC Iron for Ammonia Synthesis Based on First-Principles Theory. *ChemCatChem.* **2019**, *11*, 1928−1934.
(66) Eichler, A.; Hafner, J.; Furthmüller, J.; Kresse, G. Structural and electronic properties of rhodium surfaces: an ab initio approach. *Surf. Sci.* **1996**, *346*, 300−321.
(67) Hausleitner, C.; Hafner, J. Hybridized nearly-free-electron tight-binding-bond approach to interatomic forces in disordered transition-metal alloys. II. Modeling of metallic glasses. *Phys. Rev. B* **1992**, *45*, 128.
(68) Tománek, D.; Mukherjee, S.; Bennemann, K. H. Simple theory for the electronic and atomic structure of small clusters. *Phys. Rev. B* **1983**, *28*, 665−673.
(69) Robertson, I. J.; Payne, M. C.; Heine, V. Multi-Atom Bonding in Aluminum over a Wide-Range of Coordination-Number. *Europhys. Lett.* **1991**, *15*, 301−306.
(70) Calle-Vallejo, F.; Loffreda, D.; Koper, M. T.; Sautet, P. Introducing structural sensitivity into adsorption-energy scaling relations by means of coordination numbers. *Nat. Chem.* **2015**, *7*, 403−10.
(71) Calle-Vallejo, F.; Tymoczko, J.; Colic, V.; Vu, Q. H.; Pohl, M. D.; Morgenstern, K.; Loffreda, D.; Sautet, P.; Schuhmann, W.; Bandarenka, A. S. Finding optimal surface sites on heterogeneous catalysts by counting nearest neighbors. *Science* **2015**, *350*, 185−9.
(72) Calle-Vallejo, F.; Martinez, J. I.; Garcia-Lastra, J. M.; Sautet, P.; Loffreda, D. Fast prediction of adsorption properties for platinum nanocatalysts with generalized coordination numbers. *Angew. Chem., Int. Ed.* **2014**, *53*, 8316−9.
(73) Ma, X.; Xin, H. Orbitalwise Coordination Number for Predicting Adsorption Properties of Metal Nanocatalysts. *Phys. Rev. Lett.* **2017**, *118*, No. 036101.
(74) Wu, D.; Dong, C.; Zhan, H.; Du, X. W. Bond-Energy-Integrated Descriptor for Oxygen Electrocatalysis of Transition Metal Oxides. *J. Phys. Chem. Lett.* **2018**, *9*, 3387−3391.
(75) Nørskov, J. K.; Studt, F.; Abild-Pedersen, F.; Bligaard, T. *Fundamental concepts in heterogeneous catalysis*. John Wiley & Sons: 2014.
(76) Wells, R. H.; Gu, X.-K.; Li, W.-X.; Skodje, R. T. Understanding Surface Catalyzed Decomposition Reactions Using a Chemical Pathway Analysis. *J. Phys. Chem. C* **2018**, *122*, 28158−28172.
(77) Wang, S.; Temel, B.; Shen, J.; Jones, G.; Grabow, L. C.; Studt, F.; Bligaard, T.; Abild-Pedersen, F.; Christensen, C. H.; Nørskov, J. K. Universal Brønsted-Evans-Polanyi Relations for C−C, C−O, C−N, N−O, N−N, and O−O Dissociation Reactions. *Catal. Lett.* **2011**, *141*, 370−373.
(78) Chen, C.; Jian, M.; Liu, J.-X.; Li, W.-X. Understanding the effect of the exchange-correlation functionals on methane and ethane formation over ruthenium catalysts. *Chin. J. Chem. Phys.* **2022**, *35*, 619−628.
(79) Perdew, J. P.; Burke, K.; Ernzerhof, M. Generalized Gradient Approximation Made Simple. *Phys. Rev. Lett.* **1996**, *77*, 3865−3868.
(80) Hammer, B.; Hansen, L. B.; Nørskov, J. K. Improved adsorption energetics within density-functional theory using revised Perdew-Burke-Ernzerhof functionals. *Phys. Rev. B* **1999**, *59*, 7413.
(81) Perdew, J. P.; Wang, Y. Accurate and Simple Analytic Representation of the Electron-Gas Correlation-Energy. *Phys. Rev. B* **1992**, *45*, 13244−13249.
(82) Falsig, H.; Shen, J.; Khan, T. S.; Guo, W.; Jones, G.; Dahl, S.; Bligaard, T. On the Structure Sensitivity of Direct NO Decomposition over Low-Index Transition Metal Facets. *Top. Catal.* **2014**, *57*, 80−88.
(83) Nørskov, J. K.; Bligaard, T.; Logadottir, A.; Bahn, S.; Hansen, L. B.; Bollinger, M.; Bengaard, H.; Hammer, B.; Sljivancanin, Z.; Mavrikakis, M.; Xu, Y.; Dahl, S.; Jacobsen, C. J. H. Universality in Heterogeneous Catalysis. *J. Catal.* **2002**, *209*, 275−278.

https://doi.org/10.1021/jacs.4c01524
J. Am. Chem. Soc. 2024, 146, 8737−8745